Pergamon

Cement and Concrete Research 32 (2002) 865–879

CEMENT AND CONCRETE RESEARCH

Sodium silicate-based, alkali-activated slag mortars Part I. Strength, hydration and microstructure

A.R. Brough*, A. Atkinson

Department of Materials, Imperial College, Prince Consort Road, London SW7 2BP, UK

Received 3 January 2000; accepted 10 December 2001

Abstract

Alkali activation of ground granulated blast furnace slag (GGBFS) with sodium silicate gave clinker-free binders, with high strength and early strength development, although set times were short and somewhat variable. Isothermal calorimetry detected three heat evolution peaks (wetting, gelation of activator and bulk reaction of slag). X-ray diffraction (XRD) showed no crystalline products. Hydration was investigated by scanning electron microscopy (SEM; with quantitative image analysis) and ^{29}Si magic angle spinning nuclear magnetic resonance (MAS NMR). From early age, a uniform gel filled the initially water-filled space, and gradually densified as reaction proceeded. Microanalysis of outer product (OP) showed an Al-substituted C–S–H gel phase of widely variable (0.5–1.0) Ca/Si ratio. NMR showed long-chain substituted C–S–H with Al/Si ratio rising to 0.19 at 1 year, and also cross-linked material, consistent with a Ca- or Al-modified silica gel. Inner product (IP) regions around slag grains probably also contained hydrotalcite. Activation with KOH gave more rapid reaction of slag than for silicate activation, a less homogeneous microstructure, and lower strengths. The hydrates contained a substituted C–S–H gel of low Ca/Si ratio probably mixed with hydrotalcite, and occasional higher Al regions in the OP regions.

Keywords: Alkali-activated cement; Granulated blast furnace slag; Calorimetry; SEM; NMR

1. Introduction

Ground granulated blast furnace slag (GGBFS) has latent hydraulic properties giving rise to its extensive use as a partial replacement for Portland cement, where it is activated by alkali and lime generated by the Portland cement hydration. It can also be activated directly with alkali salts to give a clinker-free binder. Such alkali-activated slag (AAS) materials have been used in China, Eastern Europe, Scandinavia, and the former USSR; they are discussed in two extensive reviews [1,2]. Durability has sometimes been reported to be good [3], though often full details of the concrete or of additives such as retarders used in the formulations have not been given, and so it is difficult to assess the significance of the reported results.

Activation with sodium silicate (waterglass) has been widely reported to give rise to rapid hardening and high compressive strengths [4–14]. The sodium silicate-based formulation used in this paper is based upon that recommended by Wang et al. [12] who also summarised work in China [13] and elsewhere [14]. Problems, however, can be experienced with very short set times and subsequent shrinkage [15,16], and the activators used are often highly corrosive and would be difficult to handle safely outside of the laboratory. In the work described in this paper, a modified form of Wang et al.'s recommended formulation has been used [17]. The activator is a sodium silicate with higher modulus (silica-to-alkali ratio) that is less corrosive and thus safer, and which also partly alleviates the set time difficulties. Further work has been carried out at Leeds [18] where a suitable retarder for this formulation has been developed, and workable concretes have been produced and characterised.

Early-age hydration was characterised by calorimetry. Later-age hydration was quantified by image analysis and by ^{29}Si magic angle spinning nuclear magnetic resonance (MAS NMR). Compositions were determined by microanalysis in the scanning electron microscopy (SEM), and Al/Si ratios in the C–S–H from the ^{29}Si MAS NMR spectra. The effects on hydration of retarder, grinding aid, temperature, and fineness of grinding were characterised. Limited studies of a system activated with 5 M KOH provide a link to previous studies of C–S–H structure using this activator [19,20]. Chloride diffusion and binding experiments are in

* Corresponding author. Present address: Departments of Civil Engineering and Materials, University of Leeds, Leeds LS2 9JT, UK. Tel.: +44-113-233-2306; fax: +44-113-233-2265.

E-mail address: a.r.brough@leeds.ac.uk (A.R. Brough).

0008-8846/02/$ – see front matter
PII: S0008-8846(02)00717-2

Table 1
Particle size distributions (determined by light scattering) for the reference production slag and the OPC

Size/μm	Bulk slag	OPC
>40	8	17
20–40	23	24
10–20	22	17
<10	47	42

progress and will be reported later [21], as will companion studies on a range of slags with varying compositions and quenching methods [22]. The effects of admixed sodium chloride on the hydration rate [23] and corrosion of steel [24] are reported elsewhere.

2. Experimental

In this study, several different slags ground from the same batch of granulate were used. Large samples of a production slag (Appleby Group, Scunthorpe, UK) and a production OPC (Rugby Cement) were used as the main reference materials, and three laboratory grinds of the same granulate were studied to look at the effect of particle size. Particle size distributions measured by light scattering for the production cement and slag are given in Table 1. Blaine fineness for the materials were as follows: Production Slag 428, Laboratory Grinds, 332, 425, and 545. The Class M sand used to make mortars was obtained from Bawton (North Notts, UK). Samples were prepared using only the 300- to 600-μm fraction sieved from this sand in order to simplify the image analysis procedure. Unless stated otherwise, all mixes were activated with 1.5 M $(Na_2O)(SiO_2)_2$ solution (modulus = 2). Mix proportions of 0.5ml:1g:2.33g solution:slag:air-dried sand were used. The solids were premixed for 1 min, the solution was then added, and the mortar mixed for a further 2 min at slow speed in a planetary mixer. The bowl was then scraped down, and the mortar mixed for a further 1 min at fast speed and 1 min at slow speed. The samples were cast into appropriate moulds, consolidated, and cured in a humidistat at 20 °C and >95% relative humidity (RH). Samples for microscopy were sectioned so the fields of view had been horizontal during setting, and were then freeze-dried and stabilized by vacuum impregnation with a low-viscosity epoxy resin. Backscattered images were acquired from carbon-coated polished specimens, image analysis was used to determine the extent of reaction of the slag, and the solids compositions were determined by energy-dispersive X-ray (EDX). The microscopy procedures have been described in detail previously [25].

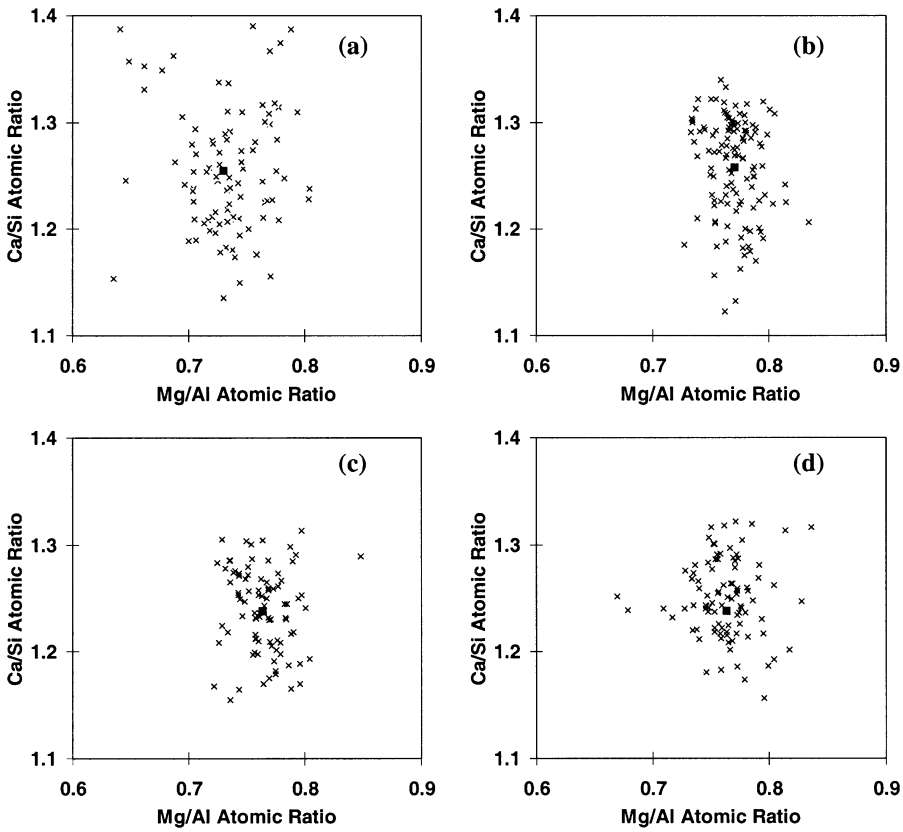

Fig. 1. Compositional variation in the ground slags. (a) Production Slag. Laboratory samples ground to various fineness. (b) 332 Blaine. (c) 425 Blaine. (d) 545 Blaine. Crosses denote individual analyses. Dark squares indicate bulk (XRF) analyses for each sample.

Table 2
Percentage (by weight) oxide compositions of the bulk slags by XRF

	Na_2O	MgO	Al_2O_3	SiO_2	K_2O	CaO	TiO_2	MnO	Fe_2O_3	BaO
Scunthorpe production	0.22	7.94	13.04	35.44	0.36	40.19	0.55	0.35	0.60	n/a
Scunthorpe laboratory grinds	0.16	8.01	12.85	35.45	0.38	40.54	0.53	0.33	0.75	0.10

n/a indicates not available.
P_2O_5, V_2O_5, Cr_2O_3, ZrO_2, ZnO, and SrO were determined at less than 0.05%.

Samples for compressive strength were cast in 160×16× 16-mm prism moulds, demoulded for 1 day, and carefully sawn into cubes. The cubes were stored in sealed plastic bags in a chamber at >95% RH until tested. The compression tests were performed by applying load between the two cast surfaces that were vertical during casting, and the cube dimensions were measured with vernier callipers to enable strength calculation. Each strength determination quoted was the average of three specimens from the same cast. Companion samples for image analysis were cast in plastic centrifuge tubes, and stored in the same chamber. The presence of some air bubbles was discovered in an initial batch of samples, despite careful consolidation to remove any air that had been entrained into the solids during mixing. To overcome this problem, it was necessary to avoid use of an Al mixing paddle that reacted with the alkaline solution.

Set times were measured on paste at the given solution-to-solids ratio using a Vicat apparatus. The paste was not adjusted to standard consistency prior to the test.

^{29}Si MAS NMR spectra were obtained at 59.63 MHz by Dr. A. Aliev (ULIRS, University College, London, UK) using a Bruker MSL300 spectrometer. MAS was performed at 4–5 kHz, relaxation delays were 5 s, and 45° pulses were used to minimise saturation (the relaxation times are relatively low due to the high levels of paramagnetic species in these systems).

Samples of paste for calorimetry (20 g of slag, 10 ml of solution) were equilibrated to temperature, mixed by hand for 5 min in a plastic bag, and then transferred to a Wexham Springs conduction calorimeter at 20 or 40 °C. A guard ring compensated for small fluctuations in water bath temperature. The system took up to 30 min to reach equilibrium after assembly, so heat output occurring during this initial time period was not recorded.

X-ray diffraction (XRD) was performed on powdered specimens using a Philips powder diffractometer with CuKα radiation. A zero background substrate was used to hold the samples.

Mortar specimens for loss on ignition (LOI) were first dried for 24 h at 105 °C, and then fired at 1000 °C for 18 h. Three determinations of approximately 5 g were used for each specimen to ensure reasonable sampling. The specimens were not ground prior to LOI determination.

3. Results

3.1. Characterisation of anhydrous slag—local glass compositions and crystallinity

The production and laboratory ground samples of slag were found to be fairly homogeneous as shown by plots of microanalyses (Fig. 1), indicating that no significant phase separation had occurred in the anhydrous slag at the scale of the microanalysis probe (~ 1 μm). Compositional data are given in Tables 2 and 3. No significant amounts of crystalline material were found in the slags by XRD analysis, indicating that they were predominantly glassy, which is consistent with the SEM observations. The broad peak due to glass could be clearly seen, falling between 27° and 34° 2θ. After hydration, relics of grains containing crystalline material were occasionally observed by SEM, but they were relatively infrequent. The ^{29}Si MAS NMR spectrum for the anhydrous slag is shown in Fig. 13 (bottom plot). The peak at -75 ppm is relatively broad, consistent with silicate species in a disordered glassy environment. The lack of any sharper components indicates that significant amounts of crystalline material are not found in this slag, or that, if present, they have long relaxation times.

Table 3
Glass composition as measured by EDX for the various slag samples, atomic ratios unless stated

Slag sample identity	Ca/Si	Al/Si	Mg/Al	Mg/Ca	Mg/Si	Ti/Ca	(Ca+Mg)/(Al+Si)	(Na+K)/Ca	S/Ca
Scunthorpe production	1.25	0.43	0.73	0.25	0.31	0.011	1.10	0.028	0.038
Scunthorpe 425 Blaine	1.24	0.42	0.76	0.26	0.32	0.011	1.10	0.029	0.040
Scunthorpe 545 Blaine	1.25	0.43	0.76	0.26	0.32	0.010	1.10	0.027	0.038
Scunthorpe 332 Blaine	1.26	0.43	0.77	0.26	0.33	0.010	1.11	0.028	0.039

For the major elements, Ca, Si, Mg, and Al, standard errors were less than 0.5% of the total amount for the element concerned. Thus, the ratios have standard errors of less than 1% of their values. For the minor elements, standard errors were larger, but generally less than 10% of the actual value.

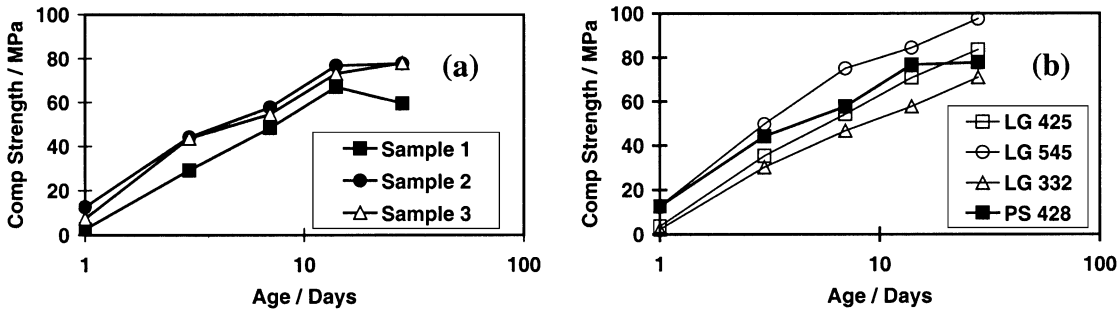

Fig. 2. Scunthorpe slag with 1.5 M waterglass (modulus = 2), 0.5 ml/g. Variability of the strength development. (a) Three mixes with the same batch of production slag. (b) Effect of fineness of laboratory grinds. LG, laboratory grind; PS, production slag. Number indicates Blaine fineness.

3.2. Activation with waterglass at room temperature

3.2.1. Set times

For the mix activated with 1.5 M (modulus = 2) waterglass and production slag, a wide variability was observed in the setting behaviour, with initial set times in the range from 2.75 to 4.25 h, and final set times in the range from 3.25 to 5.5 h. The variation was seen both within and between batches of the slag.

3.2.2. Strength development

The strengths are high in comparison with equivalent OPC mixes. There is a large amount of variability from mix to mix even within a single batch of slag, as illustrated for the reference mix using production slag (Fig. 2a). The early-age strength development seems to vary considerably, with a subsequent relatively even rate of logarithmic increase thereafter. Similar variability of behaviour both within and between batches has also been observed by coworkers at Leeds [18].

The degree of change seen, however, for the various different fineness of laboratory ground slags was much larger than the statistical sample-to-sample variability, as shown in Fig. 2b with over 20 MPa extra strength seen at 28 days for the finer grind. The laboratory grinds did not seem to have the same variable or lowered 28-day strengths as seen for the production material.

The effect of adding malic acid retarder [18] is clear (Fig. 3) with a lower strength at 1 day and thereafter. It was also suspected that the variability in setting behaviour of the production slag might be due to uneven distribution of traces of grinding aid acting as an adventitious retarder. However, when the slag was mixed with a large quantity of grinding aid added at 0.5 wt.% (Fig. 3), the addition only retarded the reaction slightly. Thus, an uneven distribution of traces of grinding aid is unlikely to account for the larger variability seen between individual batches of the production material.

3.2.3. Calorimetry

After an observed, but not quantified, initial peak due to heat of wetting, which is distorted in the period before the calorimeter cells equilibrate, two major heat evolution peaks were observed: the first at 2–3 h, and the second at around 30–40 h. The first peak corresponds roughly to the time of set, and the second peak with the onset of development of strength. The exact timings and the set times vary with different batches of slag; two typical examples are shown in Fig. 4a. The integrated heat outputs of the two peaks are unaffected by the timing, as shown in Fig. 4b, indicating that only the kinetics of the hydration changes. The basic mechanism of the hydration reaction is not changed. In the presence of malic acid retarder, both peaks are delayed [18,23]. Additions of NaCl accelerate at low levels and retard at higher levels [23].

We have also investigated the effect of sodium silicate concentration and modulus on the heat output at early age. The heat for gelation at early age (Fig. 5) appears to depend on the concentration of silica in the system, presumably reflecting the gelation of the dissolved silica to give calcium silicates. The rate at which reaction occurs is strongly influenced by the modulus of the solution. This is probably because the modulus affects the pH of the solution, and thus the rate of dissolution of anhydrous slag.

In all three cases, the main setting peak occurring at later age is less affected by the solution composition, simply being accelerated somewhat for higher soda concentration, as might be expected if the silicate were precipitated during the gelation stage.

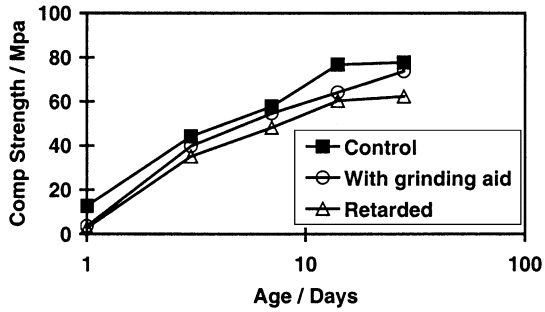

Fig. 3. Scunthorpe production slag with 1.5 M waterglass (modulus = 2), 0.5 ml/g. Effect of retarder or grinding aid.

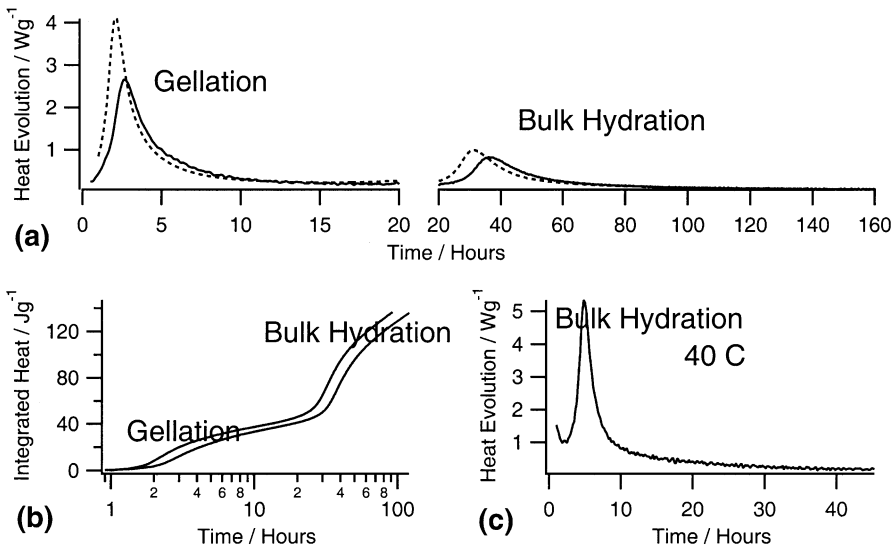

Fig. 4. Conduction calorimetry. (a) Rate of heat output for two different samples of the hydrating slag at 20 °C. (b) Integrated heat output for the same two samples, and (c) heat output for the same system but samples cured at 40 °C; at this temperature, the heat peak due to gelation of the system is lost before the calorimeter cell has time to equilibrate.

3.2.4. Evolution of microstructure

After 1 day of hydration, the microstructure (Figs. 6 and 7) consists of a homogeneous gel, with no phase separation observable in the SEM. Considerable microcracking is observed, especially against the aggregate paste interface, presumably resulting from drying shrinkage that occurred during freeze drying of the sample or during specimen preparation. After 7 days of hydration, the situation is similar except that the finest anhydrous material has now completely reacted, and the hydrate is somewhat denser.

After 14 days or 1 month, further hydration has occurred, and the degree of drying shrinkage cracking is much reduced. Distinct inner product (IP) regions, generally, but not always, darker than the outer products (OPs) can be observed as rims around partially reacted anhydrous grains and in the gel where smaller slag grains have fully hydrated. Similar features were observed after 4 months and 1 year.

An equivalent OPC specimen was also observed at 1 year (Fig. 7) and gave a paste that contained a larger proportion of pores sufficiently large (>0.6 μm) to be visible in the SEM.

The degree of reaction was assessed by image analysis to determine the amount of slag remaining (Table 4). For each sample, 30 or more images were studied and located randomly to ensure no operator bias. Some variability was found in the results, and will be considered further in the Discussion section. The micrographs give evidence for specimen shrinkage during preparation, so the extent of reaction may be somewhat underestimated, particularly at the early ages when shrinkage cracking was most severe.

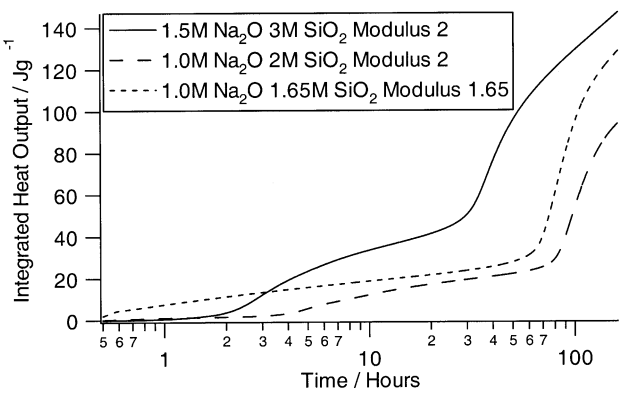

Fig. 5. Conduction calorimetry. Heat output for samples of slag hydrated with various sodium silicate solutions of different concentrations and moduli.

3.2.5. Evolution of the paste/aggregate interfacial transition zone (ITZ)

The evolution of the interfacial properties in the mortars is shown in Fig. 8. The image analysis algorithms used to obtain these data are described elsewhere [25]. Initially, the anhydrous material is packed against the sand grains, leaving a narrow interfacial zone of about 20 μm width containing less anhydrous slag than is found in the regions of bulk paste. At both 1 and 7 days, significant hydrate is found in the system, but this does not effectively fill in the interface, where a higher level of porosity than in the bulk paste is still found. To some extent, the extra space at the interface is the result of shrinkage cracking on drying for sample preparation; but nevertheless, this indicates a paste that is more porous and fragile in the region of the interface. Further hydration to 14 days leads to a system with improved microstructure, with the hydrates much more effectively filling in the space in the system. Considerable hydrate is found in

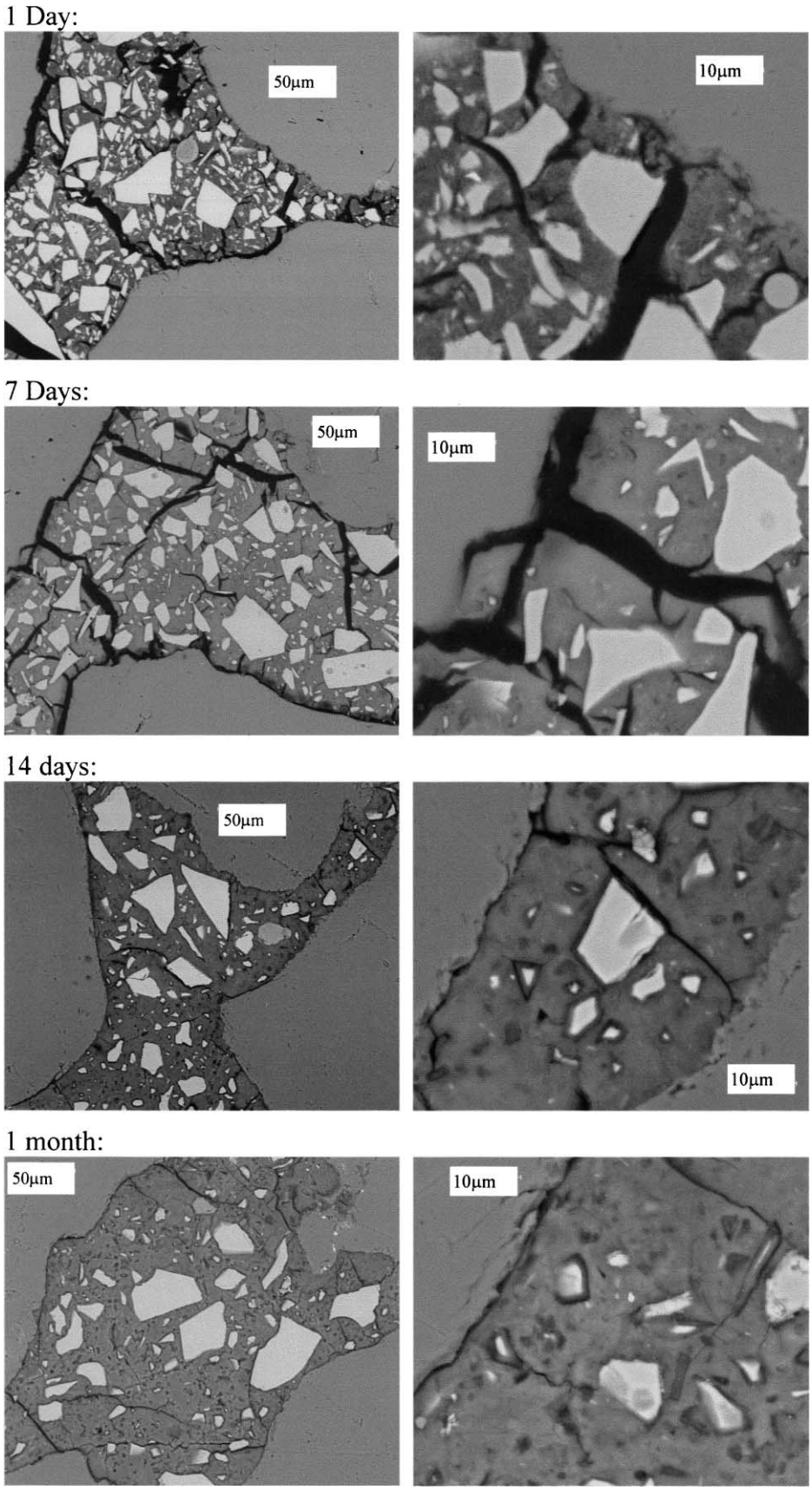
1 Day:
50μm
10μm
7 Days:
50μm
10μm
14 days:
50μm
10μm
1 month:
50μm
10μm

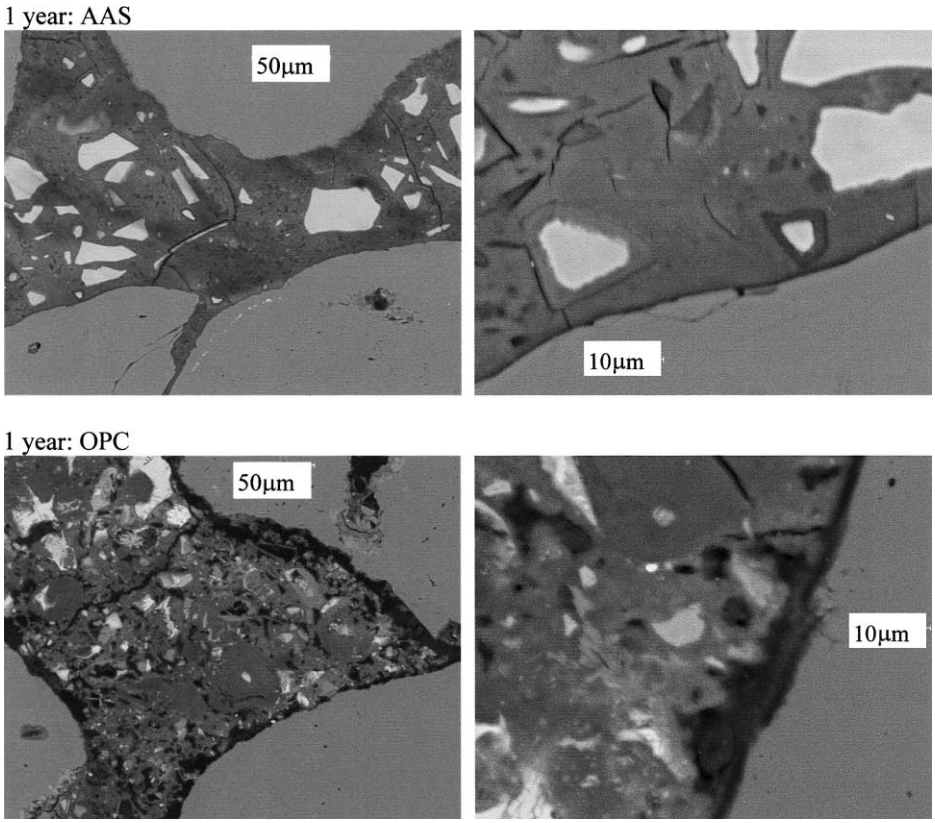

Fig. 7. Backscattered electron images of samples of OPC and of sodium silicate-activated slag mortars hydrated at room temperature at 1 year. Details as in Fig. 6.

a region where there was originally very little anhydrous slag, indicating considerable mass transport over a significant distance. Fig. 9 summarises the porosity results at 1 month of age, indicating that the AAS mortars compare favourably with OPC systems. Visual observation of Fig. 7 indicates that the waterglass AAS system has much lower interfacial porosity than the OPC system at 1 year, although we have not performed a quantitative analysis of the specimens at this age.

3.2.6. Hydration products

XRD powder diffraction was performed on the hydrated samples, and no significant peaks were observed, indicating that significant quantities of crystalline hydration products did not form in this system.

Microanalyses of the hydration products in the SEM were also performed at a range of ages. It was not possible to obtain distinct analyses from regions of different phases, indicating that the products were intermixed on the scale of the microanalysis probe (interaction volume $\sim 1\ \mu m^3$). At early age, the hydrate has a relatively low density, and the gel is relatively featureless. Hence, point analyses were performed at random across the whole sample (147 points per sample, in three grids of 7×7 points spaced by 2 μm within each grid and with the grids well separated across the sample—interfacial regions containing very little slag were avoided in these analyses). Nonetheless, a wide range of compositions was observed. Below the scale of the microanalysis probe, unreacted slag grains are embedded in the hydrate; those intersecting the surface can be seen in the BSE images (Fig. 6). There will also be grains just below the surface, not visible in the BSE images but still incorporated in the EDX analyses. Points falling within large slag grains are easily identified on the basis of their composition. It was found that calcium was very unevenly distributed throughout the hydrates at all ages, while silicon was more evenly distributed. Thus, compositional analyses were normalised relative to Si rather than Ca as is common in treatments of similar data for OPC or blended cement pastes.

Fig. 6. Backscattered electron images of samples of sodium silicate-activated slag mortars hydrated at room temperature at various ages from 1 day to 1 month. Images to left are $\times$ 400 (markers are 50 μm); images to right are $\times$ 2000 (markers are 10 μm). Black regions, porosity or cracks filled with resin; grey regions, hydrates; white material, anhydrous slag.

Table 4
Results showing extent of reaction measured by image analysis (IA) of backscattered electron images, or by LOI of mortars, or by ^{29}Si MAS NMR for 1.5 M (modulus = 2) waterglass-activated Scunthorpe production slag mortars

		Age					
Method	Raw materials	1 day	7 days	14 days	1 month	4 months	1 year
IA reaction/%	n/a	5	38	45	49	52	64
Mortar LOI/%	1.08	1.50	2.30	2.61	3.27	n/a	n/a
NMR reaction/%	n/a	16	40	n/a	61	n/a	72
KOH IA reaction/%	n/a	n/a	n/a	n/a	57	na/	n/a
KOH mortar LOI/%	1.08	2.84	3.69	n/a	4.78	n/a	n/a

Limited LOI data are also given for the KOH-activated mortars.
n/a indicates not available.

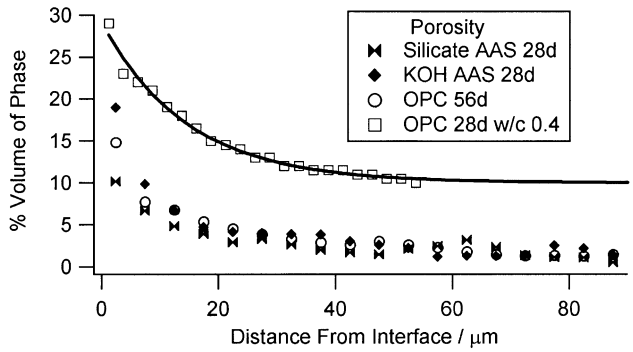

Fig. 9. Distribution of porosity in the interfacial zone (taken from Ref. [24] with permission). The image analysis procedure is such that only pores coarser than approximately 0.6 μm are measured, where this is the true pore cross-section at the point where it intersects the surface, and not the bottleneck opening as measured by MIP.

At early age, 1 day, if the hydrates consisted of a mixture of unreacted slag and sodium silicate, the analysis points in Fig. 10 would fall on the tie lines (shown as dashed lines on the graphs) between the composition for slag and for waterglass (Al/Si = Mg/Si = Ca/Si = 0). However, as shown by the arrows, the hydrates do not fall on the (dashed) tie lines due to simple admixture, but contain (relative to Si) more Al and Ca than expected at low Mg contents, and less Al and Ca than expected at high Mg contents. Mg is known not to migrate out of IP regions in OPC cements containing added slag [26]. Similar behaviour is observed here, and thus Mg can be used as a marker for IP hydrates. If it is assumed that a hydrotalcite (Mg–Al) phase forms with similar composition to that formed at later ages (see below), then this would be admixed with a silicate-containing phase having an Al/Si atomic ratio of 0.14.

Thus, in the early hydration of these systems Ca, Al, and Si migrate out of the slag regions into the OP hydrate, densifying the gelled sodium silicate. Mg remains stationary in the IP hydrate. Distinct analyses for IP hydrates are not observed, since in the BSE images at 1 day (Fig. 6), the IP rims are narrow compared with the expected EDX analysis volume. Thickening of the IP layer, rich in Al and Mg, is probably responsible for the rapid fall in long-term reaction rate.

After 1 month (Fig. 11a), a clearer formation of a hydrotalcite-like phase can be seen, admixed either with OP hydrates (left hand tie line), or with unreacted slag (right hand tie line), or with both (analyses between the two tie lines). Some analyses now have a much higher Mg/Si ratio than in the original slag, indicating that significant amounts of Si as well as Ca and Al are being removed from the slag grains. The Al/Si ratio of the OP calcium aluminosilicate gel has risen slightly to 0.17 or perhaps slightly higher.

After 1 year (Fig. 11b), there is now very clear formation of a hydrotalcite-like phase with Mg/Al ratio of 2.3. The Al/Si ratio for the OP gel is now well defined and has risen to 0.19. There are many points with Mg/Si ratio higher than

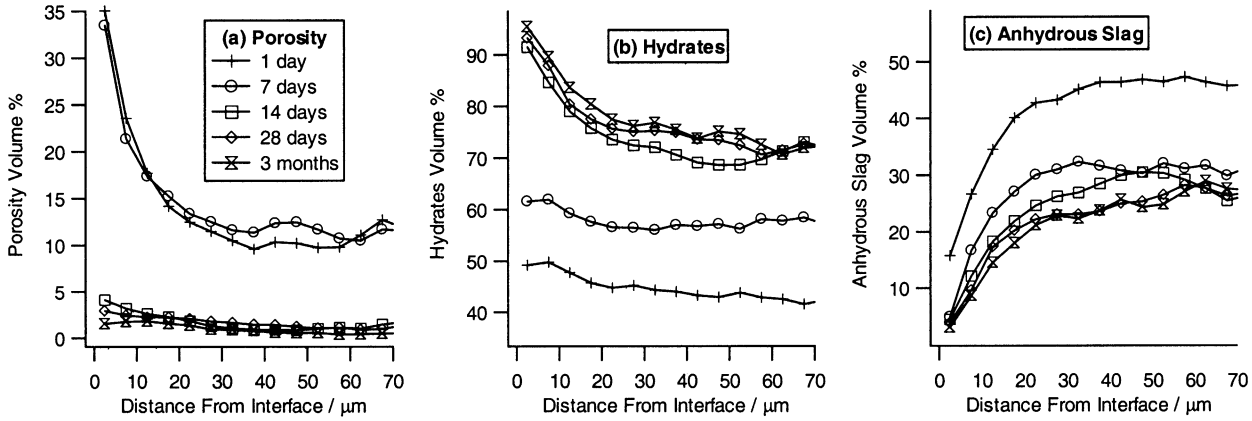

Fig. 8. Evolution of the interfacial properties of the production granulate mortar from 1 day through 3 months. (a) Porosity. (b) Hydrates. (c) Anhydrous slag. All data have standard errors of the order of 1%. Data markers are as indicated in (a).

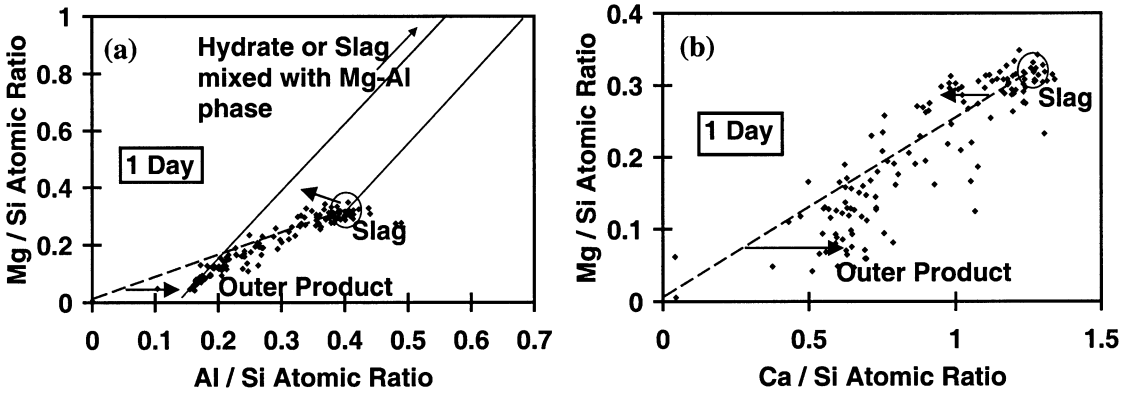

Fig. 10. Mg/Si vs. (a) Al/Si and (b) Ca/Si atomic ratios for 1- day-old samples. Dashed lines indicate tielines for mixtures of slag and waterglass. Circles indicate the composition of the unreacted slag. Solid lines indicate tie lines for mixtures of slag and OP hydrate with IP hydrate and a hydrotalcite-like phase (assuming the Mg/Al ratio observed at later ages).

the original slag grains. The gel containing the Al and Si, however, contains a variable amount of Ca since the plot of Mg and Ca ratios to Si is highly scattered (Fig. 12a), with a wide range of Ca/Si ratios from 1.2 down to 0.5. On average, OP material with low Mg had an average Ca/Si ratio of ~ 0.7, while IP material with high Mg had an average Ca/Si ratio of ~ 0.9 [Ca/(Si + Al) ratio of 0.7, allowing for Al/Si in C–S–H as determined by NMR]. Thus, material in the IP could consist of chain-like material, as in C–S–H in an OPC or OPC/slag system. In the OP material, the much lower Ca/Si ratio for many of the analysis points indicates the presence of substantial amounts of other hydrates, either Ca/Si compounds with lower Ca/Si ratio or admixed sodium silicate gel.

The presence of unreacted slag means that Mg-rich regions could contain either unreacted slag or hydrotalcite. Thus, Figs. 10a and 11 have two tie lines, and it is not possible to be sure what the IP Al/Si ratio is, since no points attributable to pure IP C–S–H and hydrotalcite are observed.

We have also investigated the distribution of Na in these systems (Fig. 12b). At early age, 1 day, this is inversely correlated with Ca content, falling roughly along the tieline from the slag composition to $Na_{0.5}Ca_{0.6}SiO_x$ (or to $Na_{0.8}SiO_x$ if extrapolated back to zero calcium content). At late age, 1 year, Na content is independent of Ca/Si ratio, with average Na/Si ratio of 0.15 for Ca/Si = 0.5 to 1.1. Thus, at early age, the Na is essentially distributed with the Si of the original sodium silicate solution, with a slightly lower-than-expected Na/Si ratio. Na/Si = 1 for the pure sodium silicate solution, but Na is prone to sublimation under the SEM beam and Na might also be easily removed during polishing, despite the use of nonaqueous media. At 1 year, when substantial reaction of slag has occurred, the Na/Si ratio is much lower due to reaction of the slag and release of additional Si into the system. No correlation is found between Na/Si ratio and Si content at 1 year, perhaps because the Na is largely present as free ions in the pore system, as suggested by Wang [27] and by work on the pore solution composition of these materials [24].

3.2.7. LOI data

LOI data for the mortars were also acquired to assess the degree of reaction. However, very high values were obtained at early ages, indicating that heating to 105 °C to

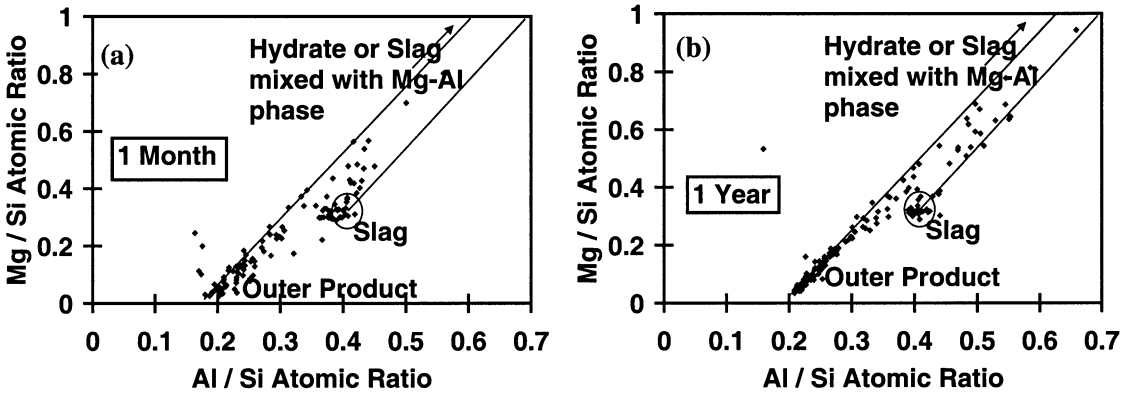

Fig. 11. Mg/Si vs. Al/Si atomic ratio plots for (a) 1-month-old and (b) 1-year-old samples. Notation as in Fig. 10.

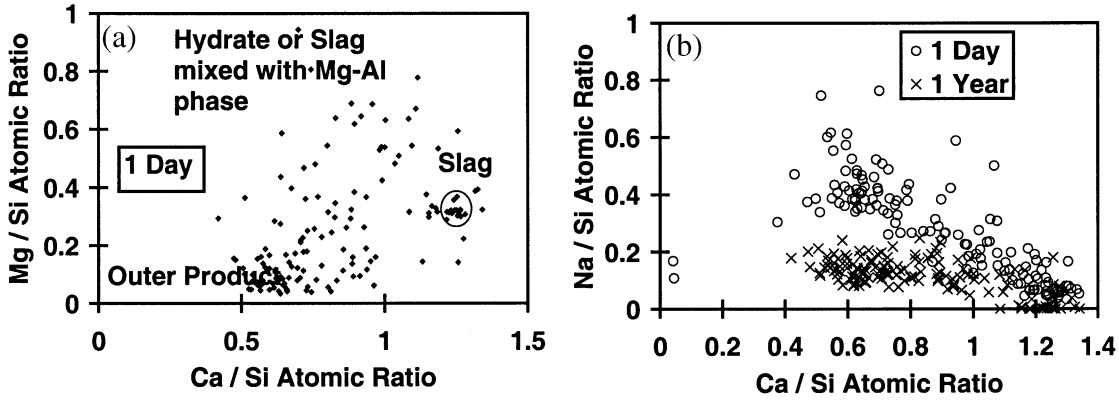

Fig. 12. (a) Mg/Si vs. Ca/Si atomic ratio plots for 1-year-old sample. (b) Na/Si vs. Ca/Si atomic ratio plots for 1-day-old and 1-year-old samples. Notation as in Fig. 10.

prepare the samples thermally activated the slag, leading to increased reaction. Thus, if LOI data are to be used reliably in these systems, the water will have to be removed by D-drying instead, so as to avoid thermal activation and reaction during the drying process.

3.2.8. ^{29}Si MAS NMR

The silicate polymerisation has been studied by ^{29}Si MAS NMR. Fig. 13 shows the spectra acquired, and Fig. 14 shows the deconvolution process, which is based on procedures written originally by Richardson et al. [19] and Brough [28] and updated more recently by Richardson and Groves [29]. The data were first fitted approximately, and then the phasing and baselines corrected carefully prior to performing the final fitting of the data. Lineshapes and positions were fitted using only the isotropic peaks. As a first approximation, first- and higher-order spinning sidebands were ignored, though care was taken to exclude these regions when fitting the baselines. The data from the anhydrous slag and the late-age, well-resolved spectra were used to aid fitting of the less well-resolved spectra acquired at earlier ages. We have not performed an analysis of errors, but the hydrate in these systems, especially the polymerised species, has much more disorder than in a conventional cement. Thus, the errors, especially for Q^{poly}, are larger.

The extent of reaction by NMR (Table 4) is somewhat larger than that estimated from image analysis. Full results from the NMR deconvolutions are given in Table 5.

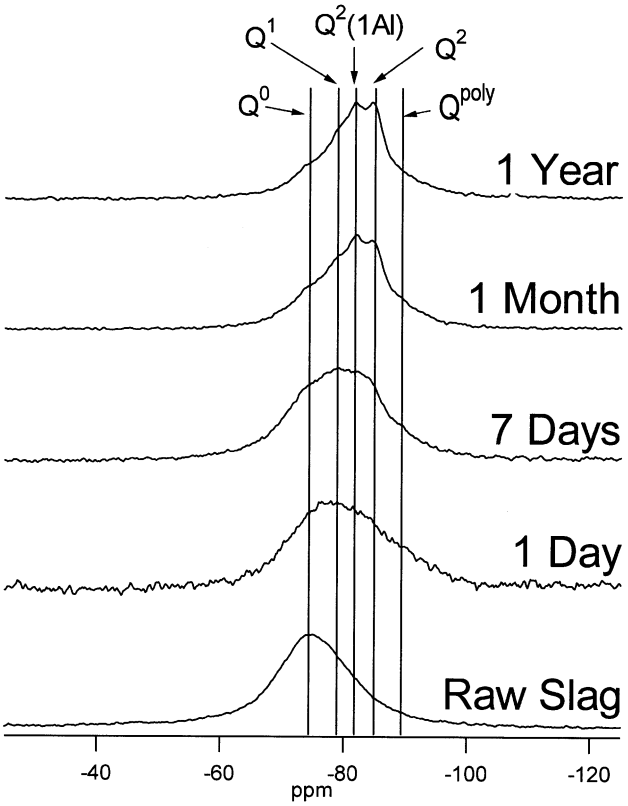

Fig. 13. ^{29}Si MAS NMR spectra of hydrating waterglass-based system with increasing hydration to 1 year.

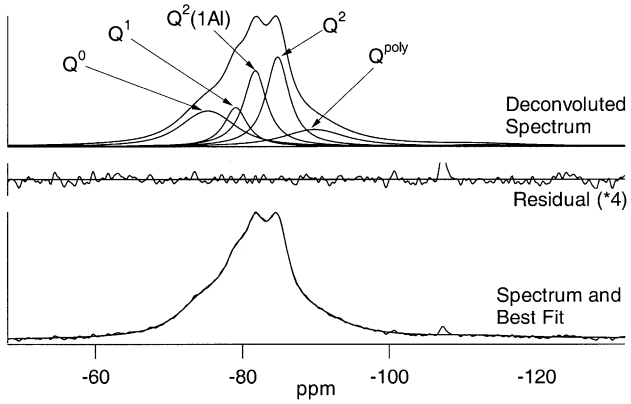

Fig. 14. ^{29}Si MAS NMR spectra for the waterglass-based system hydrated for 1 month, showing the fitted spectra and the full deconvolution and residual.

Table 5
Results of deconvolution of the NMR spectra shown in Fig. 13

Age	1 day	7 days	28 days	1 year
Species	Percentage of silicate species at this hydration time			
Q^0	67	48	31	22
Q^1	6	13	12	13
Q^2 (1Al)	2	12	22	23
Q^2	8	17	23	27
Q^{poly}	24	10	12	16
Property	Value at this hydration time			
Al/Si in C–S–H	0.06	0.14	0.19	0.18
CL	~4	~4	~5.5	~6
% Reaction slag	16	40	61	72

Q^{poly} is the estimated total for all polymerised silicate species, located in a gel phase or cross-linked within a tobermorite-based phase. Al/Si in C–S–H is the ratio of aluminate coordinated tetrahedrally in silicate chains relative to their silicate content. CL is the mean aluminosilicate chain length, not allowing for Q^{poly}, and assuming no cross-linking or chain-terminating Al.

Substantial Al is incorporated into the silicate chains, giving an Al/Si ratio of 0.2 at later ages. The aluminosilicate chains are significantly longer than for a similar age in a Portland cement system, and there is also substantial polymerised material, largely at −90 ppm, corresponding to cross-linked calcium- or aluminium-substituted silicate species. The reduction of Q^{poly} from 1 to 7 days is unambiguous, and indicates that some sodium silicates react with the Ca from the slag to form C–S–H. The subsequent rise of Q^{poly} is less certain; it could arise from some carbonation of the systems at late age (not tested for).

3.3. Hydration with waterglass at 5 and 40 °C

Strength determinations have also been performed for samples hydrated over the range of temperatures, which might occur during concreting operations (Table 6). There is a strong influence of mixing/curing temperature upon strength, with significant retardation at 5 °C and significant acceleration of strength development for 40 °C curing. The variation is larger than that seen for a typical OPC concrete [30]. The sample hydrated at 5 °C was too weak to demould at 1 day, although at 28 days it still gave reasonable strength.

3.4. Simulated steam curing—hydration at 80 °C

Samples hydrated at 80 °C to simulate steam curing were found (Table 6) to develop strength very rapidly, with 12 h of curing giving over 70 MPa—similar to the strength achieved after 28 days at room temperature. When retarder was present, lower strengths were obtained. The microstructure of the non-retarded samples (Fig. 15) is similar to that of samples hydrated at room temperature for later ages (1 month to 1 year).

3.4.1. Composition of the hydrates

The composition of the hydrates formed on curing at 80 °C (Fig. 16) is similar to those formed at room temperature (Fig. 11), with a hydrotalcite-like phase with Mg/Al ratio of approximately 2.4 admixed with calcium aluminosilicate gel with Al/Si ratio of 0.18. As at room temperature, a wide range of Ca/Si ratios was observed (plot not shown).

3.5. KOH activation

Activation with KOH gave a higher 1-day strength (Fig. 17) than activation with waterglass, but the subsequent strength development was much lower, and strengths at later ages were much lower for KOH activation relative to waterglass activation.

The LOIs are much higher than for the waterglass (Table 4) for a given age, despite the lower strengths. The degree of reaction by image analysis, measured at 1 month, was 57%, significantly higher than that for activation of the same slag with sodium silicate (40%), despite the lower strength of the KOH-activated mix.

The microstructure of the KOH-activated mix is very different from that of the waterglass-activated mortars, being much more heterogeneous (Fig. 18) with much more porosity and interfacial porosity.

The Al/Si ratio of the C–S–H (see Fig. 19) is high at ~0.25, and the C–S–H has a well-defined Ca/Si ratio of approximately 1.1, i.e., a Ca/(Si + Al) ratio of approximately 0.9 corresponding to the lower limit for a tobermorite-like C–S–H gel based on the models available [31,32]. There are a few points with low Mg content, but high Al/Si ratios, which are probably due to admixture of small quantities of C_4AH_{13} or similar phases, as suggested by Wang and Scrivener [10] for similar systems. However, we have not been able to determine significant compositional correlations for these points. The C–S–H in IP regions is admixed with a Mg–Al phase with approximate Mg/Al ratio of 2.8, probably hydrotalcite.

Table 6
Compressive strengths for mortars cubes cured for various ages at various temperatures

Hydration temperature (°C)	Compressive strength/MPa			
	1 day	3 days	7 days	28 days
5	[a]	2	7	41
20	7	44	55	78
40	52	65	79	99
80[b]	72	–	–	–
80, retarded[b,c]	46	–	–	–

[a] Strength too low to demould sample; sample demoulded at 3 days.
[b] Data for samples of mortar precured at room temperature for 4 h, and then heat treated at 80 °C for 12 h and allowed to cool slowly back to room temperature.
[c] The retarded sample contained 0.5 wt.% of slag of malic acid retarder [18].

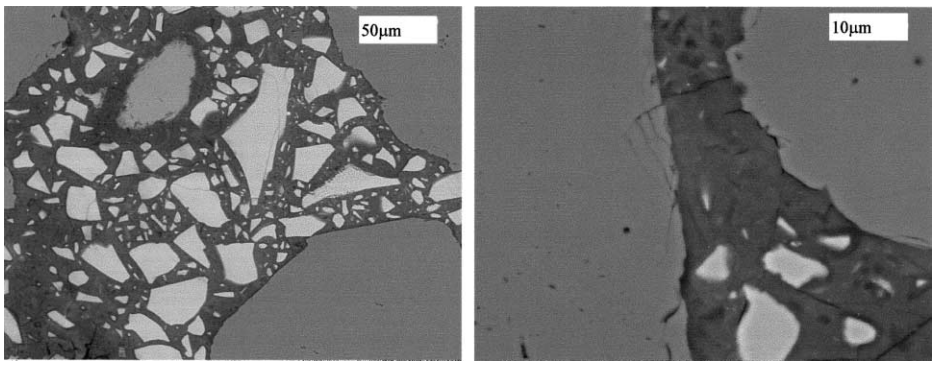

Fig. 15. Microstructure of AAS mortar precured for 4 h at room temperature, and then cured at 80 °C for 12 h. Details as in Fig. 6.

We have also investigated the ITZ in the KOH-activated system. The results are described in detail elsewhere [25]. Porosity results are summarised in Fig. 9.

4. Discussion

4.1. Extent of reaction

The image analysis data are not considered to be particularly reliable, since some drying shrinkage occurred during sample preparation for the SEM, despite freeze-drying conditions being employed. This drying shrinkage can also been seen by the extensive microcracking, especially for early age samples. We also attempted measurements on paste, but these proved impossible due to visible shrinkage occurring. This reduces the overall sample volume, while the volume of unreacted material is not altered, and thus the extent of reaction is underestimated. Indeed, the NMR data give higher extents of reaction than the image analysis data (although the NMR values could miss some of the anhydrous slag, due to the presence of paramagnetic impurities). The waterglass-activated mortar at 1 month (Table 4) gave 61% by NMR but 49% reaction by image analysis.

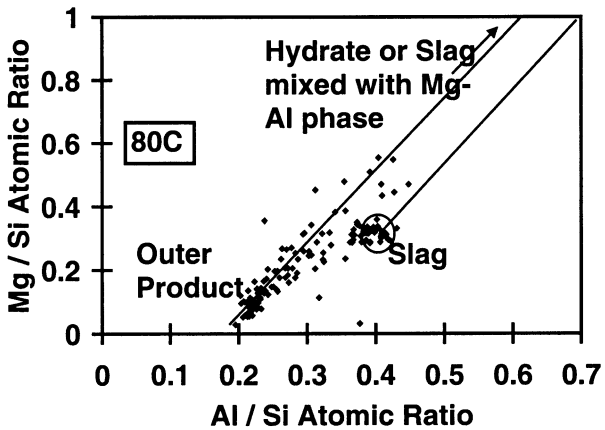

Fig. 16. Mg/Si vs. Al/Si atomic ratio plots for sample cured at 80 °C. Notation as in Fig. 10.

4.2. Strength development

While the waterglass-to-slag ratio is 0.5 ml/1 g, the solids content of the waterglass solution is 22%, and it has a density of 1.21. Thus, overall, the water-to-total solids ratio is 0.42. This is a similar ratio to that used for BS12 tests of cement strength development, where the allowable strengths at 3 and 28 days are much lower, even for rapid-hardening OPC, than those reached by these AAS pastes, e.g., for BS12:1987, the 3-day strength for OPC must be greater than 23 MPa (29 MPa RHPC) against a strength for the AAS mortars studied here of around 40 MPa. Companion work on concretes [18] has seen compressive strengths well in excess of 100 MPa, indicating the ability of this formulation to achieve very high compressive strengths.

4.3. Composition and nature of the hydrates

For the water glass-activated system, the hydrates consist of IP and OP regions containing a Mg–Al phase, presumably similar to hydrotalcite, found within the IP regions and having an Mg/Al ratio of 2.4. This is admixed with IP hydrate C–S–H. The C–S–H has an Al/Si ratio of the order of 0.06 initially rising to 0.19 at 1 year, combining the data from NMR and EDX. There is good agreement between these techniques from 7 days onwards, and the data for 1-day curing will be strongly influenced by changes taking place during drying. The Ca/Si ratio is highly variable, although on average it is higher in the IP than in the OP, which is expected, since the OP regions are filled at early age by Si-rich deposits from the gelation of the sodium silicate. Much of the OP is too Ca-deficient to be accounted for on the basis of "tobermorite like" C–S–H gel, but must instead consist of C–S–H admixed with silica gel modified with calcium and aluminium, consistent with the NMR observations of admixed cross-linked silicates.

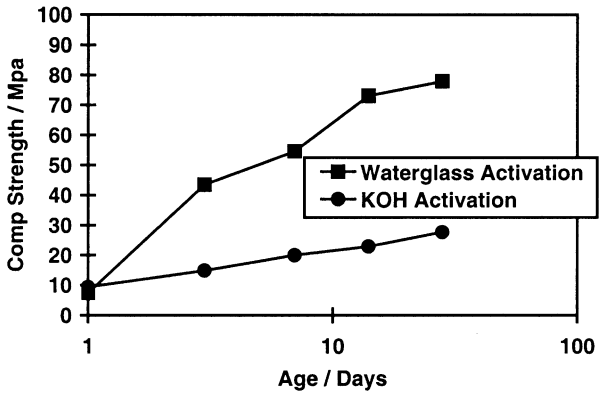

Fig. 17. Strength development. Scunthorpe production slag activated with sodium silicate or with 5 M KOH.

Similar hydrates occur in the KOH system, except that the Ca/Si ratio is less variable at about 1.1, which is within the range of composition consistent with a tobermorite-like C–S–H. There is slightly more Al substituted in the C–S–H gel and the hydrotalcite has a slightly higher Mg/Al ratio. There are also limited amounts of low silicon material with higher Al/Ca ratio, possibly related to AFm.

4.4. ITZ

The distribution of hydrates in the KOH-activated slag mortar was similar to that in the OPC cement, with considerable interfacial porosity. After 1 month of hydration, however, the hydrates in the sodium silicate-activated mortar filled space more efficiently, and gave rise to much less porosity, even though the degree of reaction of slag was much lower.

The actual water-to-cementitious solids ratio was 0.42, as calculated in the discussion of the strength results. An OPC mixed at 0.4 W/C, reported in the literature [33], contained 5% bulk porosity at 180 days by image analysis, with values in the interfacial region of up to 15%. Even when 15% silica fume was added to the OPC system and the w/c ratio reduced to 0.33 [33], the bulk porosity remained as high as 4% with increases to 7% in the interfacial zone at 180 days. The waterglass-activated mortar studied here has total porosity observed in BSE images of about 1%, rising to only 2% in the ITZ. Thus, the AAS mortar compares very favourably with both OPC and OPC/silica fume mortars of similar age.

5. Conclusions

(1) The slag samples used in this study were predominantly glassy, with very little crystalline material.

(2) High strengths were developed rapidly on activation with 1.5 M $(Na_2O)(SiO_2)_2$ solution (modulus = 2).

(3) Set times and onset of strength for alkali activation with this solution varied considerably between batches, and also from mix to mix using one batch of the slag.

(4) After the initial exotherm due to wetting of the slag, two peaks were observed in the calorimetry of this system; the first corresponds to gelation and set of the sodium silicate, and the second to bulk hydration of the slag responsible for strength development.

(5) The products of hydration with sodium silicate are amorphous and uniformly distributed throughout space in the mortars. No significant phase separation was observed at the scale of the SEM microprobe at early age. As hydration proceeded, IP regions higher in phases containing Mg and Al could be observed.

(6) These IP rims are probably responsible for eventually slowing down the reaction rate to very low values while significant hydrated slag still remains.

(7) From ^{29}Si MAS NMR at early age, the silicate gel formed by gelation of the waterglass is partly consumed to form linear-chain Al-substituted C–S–H with long chains. At later ages, extra Al is substituted into the C–S–H and additional cross-linking probably occurs.

(8) The interfacial properties of the sodium silicate-activated mortars are excellent, with low levels of porosity at the interface with aggregate.

(9) Thermal activation of the sodium silicate-activated systems is significant, and heat curing (12 h at 80 °C) can

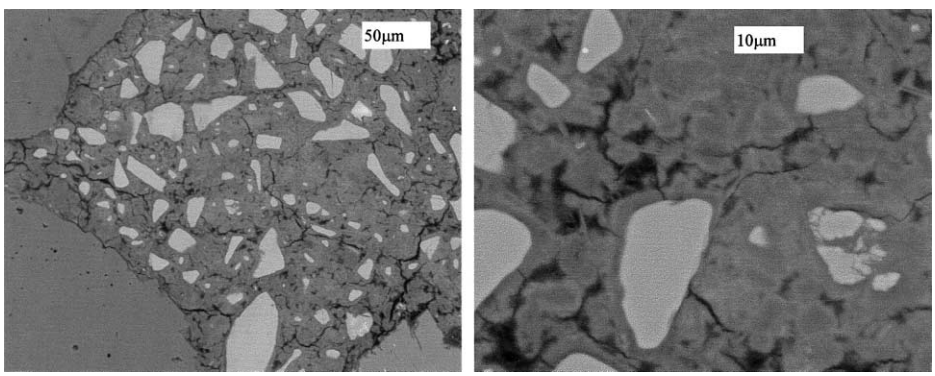

Fig. 18. Microstructure of KOH-activated AAS mortar, 1 month old. Details as in Fig. 6.

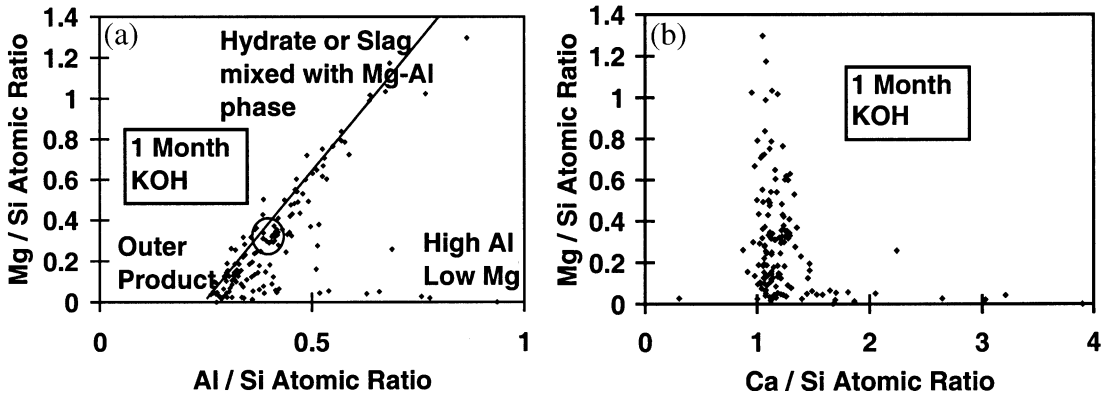

Fig. 19. Atomic ratio plots for sample hydrated with KOH solution. Mg/Si vs (a) Al/Si, and (b) Ca/Si ratio. Notation as for Fig. 10.

give rise to high early strengths, even when the system was retarded to give longer working times before initial set.

(10) LOI data give misleading estimates of the extent of reaction of the slag at early age due to thermal activation of unreacted slag during the drying to 105 °C.

(11) Image analysis of backscattered images in the SEM is unsuitable for accurately assessing the extent of reaction in these systems due to drying shrinkage during specimen preparation. This applies even when care is taken to limit this by vacuum drying from samples cooled to −20 °C.

(12) Hydration with KOH instead of waterglass gave a much more heterogeneous microstructure, with a lower strength developed for a given degree of hydration, and greater porosity both in the bulk paste and in the interfacial zone.

Acknowledgments

We thank EPSRC and the Cementitious Slag Makers Association for support under grant GR/K52201, and the EPSRC for funding equipment under grant GR/L26537. We thank Appleby Group for supply, preparation, fineness characterisation, and XRF analyses of the various slag samples; Crossfield (Warrington, UK) for the supply of waterglass samples; Dr. I.G. Richardson, Dr. D. Ou, and the late Prof. J.G. Cabrera of the University of Leeds for collaboration on various aspects of these materials; Dr. A. Aliev of the University of London Intercollegiate NMR Service for obtaining the NMR spectra; and Dr. G. Fowler for use of and help with using the calorimetry facilities at Imperial College.

References

[1] B. Talling, J. Brandstetr, Clinker free concrete based on alkali activated slag, in: S.L. Sarkar, S.N. Ghosh (Eds.), Mineral Admixtures in Cement and Concrete, vol. 7, ABI Books Private, India, 1993, pp. 296–341.

[2] D.M. Roy, Alkali activated cements: Opportunities and challenges, Cem. Concr. Res. 29 (1999) 249–254.

[3] P.M. Gifford, J.E. Gillott, Freeze thaw durability of activated blast furnace slag cement concrete, ACI Mater. J. 93 (1996) 242–245.

[4] C. Qing-Hua, A. Tagnit-Hamou, S.L. Sarkar, Strength and microstructural properties of water glass activated slag, in: F.P. Glasser, G.J. Young, J.F. Young, T.O. Mason, P.L. Pratt (Eds.), Advanced Cementitious Systems: Mechanisms and Properties, Materials Research Society, Pittsburgh, Pennsylvania, Mater. Res. Soc. Symp. Proc. vol. 245 (1992) pp. 49–54.

[5] E. Douglas, J. Brandstetr, A preliminary study of the alkali activation of ground granulated blast furnace slag, Cem. Concr. Res. 20 (1990) 746–756.

[6] E. Douglas, A. Bilodeau, J. Brandstetr, V.M. Malhotra, Alkali activated ground granulated blastfurnace slag concrete: Preliminary investigation, Cem. Concr. Res. 21 (1991) 101–108.

[7] J. Malolepszy, W. Nocun-Wczelik, Microcalorimetric studies of slag alkaline binders, J. Therm. Anal. 33 (1988) 431–434.

[8] V. Tomkova, S. Sahu, J. Majling, M. Tomko, Alkali activation of granulated blast furnace slags, Ceram.-Silik. 37 (1993) 61–65.

[9] F. Skvara, M. Kopecka, Properties of a cement based on alkali activated slag, Ceram.-Silik. 41 (1997) 29–34.

[10] S.D. Wang, K.L. Scrivener, Hydration products of alkali activated slag cement, Cem. Concr. Res. 25 (1995) 561–571.

[11] C. Shi, R.L. Day, X. Wu, M. Tang, Comparison of the microstructure and performance of alkali slag and Portland cement pastes, 9th Int. Cong. Chem. Cem. 3 (1992) 298–304.

[12] S.D. Wang, K.L. Scrivener, P.L. Pratt, Factors affecting the strength of alkali activated slag, Cem. Concr. Res. 24 (1994) 1033–1043.

[13] S.D. Wang, Review of recent research on alkali activated concrete in China, Mag. Concr. Res. 43 (1991) 29–35.

[14] S.D. Wang, X.-C. Pu, K.L. Scrivener, P.L. Pratt, Alkali activated slag cement and concrete: A review of properties and problems, Adv. Cem. Res. 7 (1995) 93–102.

[15] P.M. Gifford, J.E. Gillott, ASR and alkali carbonate reaction in activated blast furnace slag cement concrete, Cem. Concr. Res. 26 (1996) 21–26.

[16] E. Douglas, A. Bilodeau, V.M. Malhotra, Properties and durability of alkali activated slag concrete, ACI Mater. J. 89 (1992) 509–516.

[17] A.R. Brough, Unpublished results.

[18] D. Ou, I.G. Richardson, J. Cabrera, Design and engineering properties of alkali activated slag concrete, Mag. Concr. Res., submitted for publication.

[19] I.G. Richardson, A.R. Brough, R. Brydson, G.W. Groves, C.M. Dobson, Location of aluminium in substituted CSH gels as determined by ^{29}Si and ^{27}Al NMR and EELS, J. Am. Ceram. Soc. 76 (1993) 2285–2288.

[20] I.G. Richardson, A.R. Brough, G.W. Groves, C.M. Dobson, The characterisation of hardened alkali activated BFS pastes, and the nature of the CSH phase, Cem. Concr. Res. 24 (1994) 813–829.

[21] A.R. Brough, A. Atkinson, Sodium silicate activated alkali activated slag mortars. Part IV: Chloride binding and diffusion, Cem. Concr. Res., submitted for publication.
[22] A.R. Brough, A. Atkinson, Sodium silicate based alkali activated slag mortars. Part III: Effect of slag composition and quenching technique, Cem. Concr. Res., submitted for publication.
[23] A.R. Brough, M. Holloway, J. Sykes, A. Atkinson, Sodium silicate activated alkali activated slag mortars. Part II: The retarding effects of additions of sodium chloride or malic acid, Cem. Concr. Res. 30 (2000) 1375–1379.
[24] M. Holloway, J. Sykes, Corrosion of steel embedded in chloride contaminated alkali activated slag mortars, Corros. Sci., submitted for publication.
[25] A.R. Brough, A. Atkinson, Automated identification of the aggregate–paste interfacial transition zone in mortars of silica sand with Portland or alkali activated slag cement paste, Cem. Concr. Res. 30 (2000) 849–854.
[26] A.M. Harrisson, N.B. Winter, H.F.W. Taylor, Microstructure and microchemistry of slag cement pastes, in: L.J. Struble, P.W. Brown (Eds.), Microstructural Development During Hydration of Cement, Materials Research Society, Pittsburgh, Pennsylvania, Mater. Res. Soc. Symp. Proc. 85 (1987) pp. 213–222.
[27] S. Wang, Alkaline activation of slag, PhD Thesis, Imperial College, University of London, 1995.
[28] A.R. Brough, NMR studies of inorganic solids, PhD Thesis, University of Oxford, 1993.
[29] I.G. Richardson, G.W. Groves, The structure of the calcium silicate hydrate phases present in hardened pastes of white Portland cement blast-furnace slag blends, J. Mater. Sci. 32 (1997) 4793–4802.
[30] A.M. Neville, Properties of Concretes, third ed., Longman, London, 1981.
[31] H.F.W. Taylor, Proposed structure for CSH gel, J. Am. Ceram. Soc. 69 (1986) 464–467.
[32] I.G. Richardson, G.W. Groves, The incorporation of minor and trace-elements into calcium silicate hydrate (C–S–H) gel in hardened cement pastes, Cem. Concr. Res. 23 (1993) 131–138.
[33] K.L. Scrivener, A. Bentur, P.L. Pratt, Quantitative characterization of the transition zone in high strength concrete, Adv. Cem. Res. 1 (1988) 230–237.